NIR-Triggered Synergic Photo-chemothermal Therapy Delivered by Reduced Graphene Oxide/Carbon/ Mesoporous Silica Nanocookies

*Yu-Wei Chen, Po-Jung Chen, Shang-Hsiu Hu, I-Wei Chen, and San-Yuan Chen**

A novel photo-responsive drug carrier that doubles as a photothermal agent with a nanocookie-like structure is constructed by coating amorphous carbon on a mesoporous silica support self-assembled on a sheet of reduced graphene oxide. With a large payload (0.88 mmolg^{-1}) of a hydrophobic anti-cancer drug, (S)-(+)-camptothecin (CPT), nanocookies simultaneously provide a burst-like drug release and intense heat upon near-infrared exposure. Being biocompatible yet with a high efficiency for cell uptake, nanocookies have successfully eradicated subcutaneous tumors in 14 days following a single 5 min NIR irradiation without distal damage. These results demonstrate that the nanocookie is an excellent new delivery platform for local, on-demand, NIR-responsive, combined chemotherapy/hyperthermia for tumor treatment and other biomedical applications.

1. Introduction

Stimuli-sensitive drug-delivery nanosystems have attracted much attention owing to their enhanced therapeutic efficacy. An ideal system should carry a secure cargo which is released after reaching the target in response to a stimulus such as pH, temperature, redox potential, magnetic field, ultrasonic, and photo-irradiation.[1–6] Of special interest to this strategy is the delivery of drugs of low water/serum solubility. Such drugs are often carried by liposomes and micelles, which have a hydrophilic outer shell and a hydrophobic inner compartment, the latter suitable for hydrophobic cargo. But these vehicles are known to suffer from relatively poor stability. Here we demonstrate a biocompatible, photo-irradiation responsive, cell-penetrating, large-payload, inorganic nanocomposite that functionally emulates liposomes and micelles, but with superior stability and responsivity. This nanocomposite, made of mesoporous silica (hydrophilic, cell penetrating), amorphous carbon (hydrophobic, drug carrying, large payload) and reduced graphene oxide (rGO, hydrophilic, photo-sensitive), has been injected into mouse models to deliver an anticancer drug, (S)-(+)-camptothecin (CPT), to tumors, where a burst-like drug release is externally triggered by near infrared (NIR) exposure, which simultaneously causes hyperthermia.

Mesoporous silica nanostructure (MSN) is potentially an excellent drug carrier with high thermal stability, tunable pore size, large loading capacity, biocompatibility, and easy surface modification.[7] However, the drawback of unmodified MSN is easy drug leak from the open silica pore, resulting in side effect to normal cells.[8–10] On the other hand, amorphous carbon, which is like MSN, has high specific surface area and biocompatibility, can absorb hydrophobic molecules strongly, which will improve the success of anticancer drug to cancer cells. Meanwhile, rGO which displays excellent photon-to-thermal-energy transfer efficiency under NIR irradiation has been used for photothermal therapy in vitro,[11,12] and in vivo,[13] and for combined photothermal therapy and chemotherapy (with doxorubicin) in vivo.[14] To date, such efforts to seek combined rGO-based phototherapy and chemotherapy rely upon the standard approach of coating the drug carrier (rGO) with biocompatible linker polymers (e.g., PEG[12–14] and glucose[15]). However, this approach has the shortcomings of (i) drug release being hampered by coating which is a diffusion barrier,[16] and (ii) NIR absorption being reduced by coating which is an optical barrier. This has severely limited the efficacy of rGO-drug for tumor treatment.[17] In this work, we seek to unobtrusively co-arrange MSN and amorphous carbon on an rGO "cookie sheet", thereby combining high efficiency photothermal therapy and on-demand rapid chemotherapy (**Scheme 1**).

Y.-W. Chen, Dr. P.-J. Chen, Prof. S.-Y. Chen
Department of Materials Sciences and Engineering
National Chiao Tung University
Hsinchu, 300, Taiwan
E-mail: sanyuanchen@mail.nctu.edu.tw
Prof. S.-Y. Chen
Material and Chemical Research Laboratories
Industrial Technology Research Institute
195, Sec. 4, Chung Hsing Rd., Chutung
Hsinchu, Taiwan, 31040, R.O.C.
Prof. I.-W. Chen
Department of Materials Sciences and Engineering
University of Pennsylvania
Philadelphia, PA 19104-6272, USA
Prof. S.-H. Hu
Department of Biomedical Engineering
and Environmental Sciences
National Tsing Hua University
Hsinchu, 300, Taiwan

DOI: 10.1002/adfm.201301763

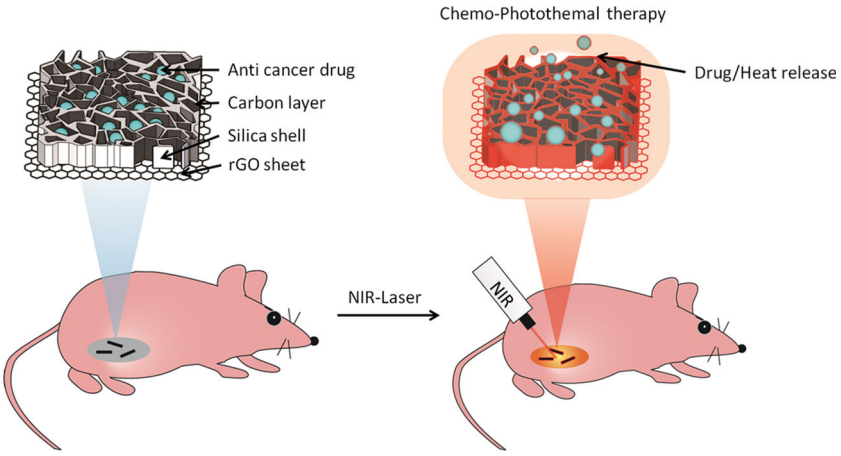

Scheme 1. Schematic illustration of chemo-photothermal therapy using reduced graphene oxide/carbon/mesoporous silica nanocookies, under NIR light-control.

2. Results and Discussion

This low-cost, low toxicity construct can be produced using the facile preparation method schematically illustrated in **Figure 1**, in which rGO is used as the substrate of the nanocomposite. To enhance cell uptake, we selected a small sized (141 nm) rGO, which was obtained by sonication and centrifugation following a modified Hummers method.[18] To template MSN growth, a cationic surfactant (cetyltrimethyl ammonium bromide, CTAB) was first absorbed onto the surface of rGO by electrostatic interactions between the cationic head group of CTAB and the anionic group of rGO. MSN with pore channels was next grown by controlled hydrolysis of tetraethylorthosilicate (TEOS) *via* a micelle mechanism that involved CTAB as a surfactant.[19] To incorporate carbon into the composite, we first simultaneously formed polystyrene by polymerizing (using an initiator, *n*-octane,2,2′-azobis(2-amidinopropane) dihydrochloride (AIBA)) styrene monomers inside the pore channels during MSN formation. We next sulfonated and then pyrolyzed polystyrene in high temperature argon to form carbon deposit on the channel wall. This nanocomposite will be named "nanocookie." For comparison, a similar composite but having no carbon, called rGO/PSS (PSS stands for porous silica sheet), was prepared without styrene (see Figure 1), and another construct having no rGO and carbon, called PSS, was prepared by pyrolyzing in air (Figure 1). The intermediate product, without sulfonation and pyrolysis, called rGO@SS, was also studied (Figure 1).

According to dynamic light scattering, the average rGO size is 141 nm; other products all have a similar size as shown in **Table 1**. Scanning electron micrographs (SEM) shown in **Figure 2**a confirm the size determination. In addition, they found rGO@SS displayed an irregular sheet morphology. There are no visible pores in these sheets according to transmission electron microscopy (TEM), Figure 2b, which is consistent with their polymer/organic (fill) content in this construct. In comparison, nanocookies shown in Figure 1c (SEM) have a relatively well-defined thickness of 35 nm and are partitioned into cells (due to MSN channels) of ~5 nm size (inset of Figure 1d, TEM). This was confirmed by measuring specific (BET) surface area using nitrogen absorption/desorption isotherms, which found nanocookies with a surface area of ~720 m^2 g^{-1} and an average pore size of 5 nm.

Other products all have a similar particle size indicating that the rGO substrate is rather robust (Table 1). Nevertheless, the pore size of different products differs considerably. In particular, whereas the pores of nanocookie and PSS (5 nm) are the same, they are much larger than those of rGO@PSS (1.8 nm). Referring to Figure 1, we believe this indicates that the diameter of the MSN channel was considerably enlarged by incorporating styrene/polystyrene. This is in agreement with the results of Nandiyanto *et al*. who found pore size expansion, from 5 nm to 15 nm, as the styrene concentration increased.[20] We also note that SEM and TEM did not reveal any free silica or polystyrene particle, indicating that silica and polystyrene were homogeneously distributed during (wet) preparation without phase separation despite their entirely different hydrophilicity/hydrophobicity. This indicates that our CTAB templating method, which allowed densely packed micelles to form, was apparently successful for co-packaging silica and polystyrene (as carbon precursor) into the micelles.

The existence of polystyrene in rGO@SS was confirmed by Fourier-transform infrared (FT-IR) spectra in **Figure 3**a. Vibrational

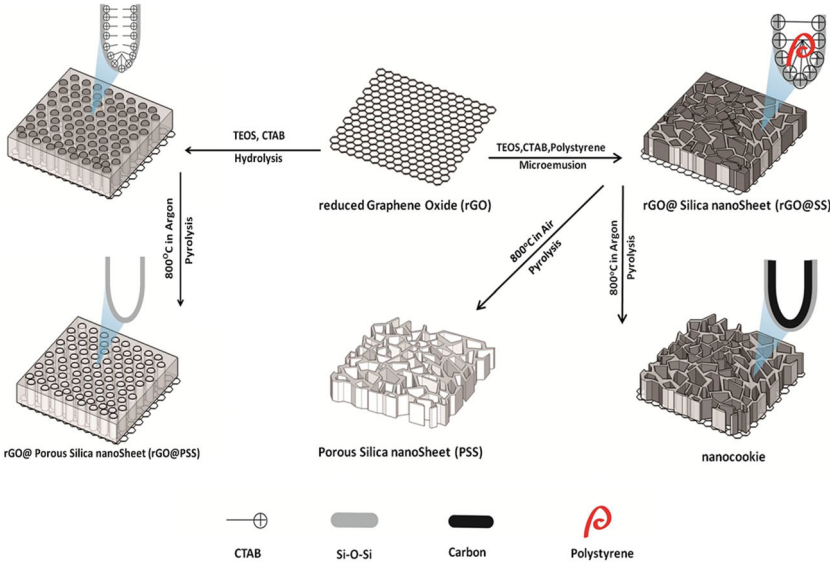

Figure 1. Schematic illustration of synthesis and microstructure of reduced Graphene Oxide (rGO), Porous Silica nanoSheet (PSS), rGO@Silica nanoSheet (rGO@SS), rGO@Porous Silica nanoSheet and nanocookie.

Table 1. Structural parameters of rGO, nanocookie, rGO@PSS and PSS.

Structure type	Particle size [nm][a)]	S_{BJH} [m^2/g][b)]	V_{BJH} [cm^3/g][b)]	Pore size [nm][b)]
rGO	~141	417.36	0.63	~3.6
nanocookie	~162	723.26	0.59	~5
rGO@PSS	~157	817.63	0.68	~1.8
PSS	~151	1019.15	0.91	~5.1

[a)]From dynamic light scattering (DLS); [b)]Mesopore surface area (S_{BJH}) and mesopore volume (V_{BJH}) calculated by the BJH model from the BET absorption/desorption data.

peaks of polystyrene (aliphatic C–H stretching at approximately 2820–2967 cm^{-1}, aromatic C–H stretching at 2994–3043 cm^{-1}, and C–C stretching in aromatic ring at 1500 cm^{-1}) only appear in rGO@SS.[21] The absorptions at 1637 cm^{-1} and 800 cm^{-1} correspond to moisture, which came from atmosphere.[22] The peaks at ~1100–1200 cm^{-1} are attributed to the Si–O–C/Si–O–Si and the ones at ~3450 cm^{-1}, ~1100 cm^{-1} and ~950 cm^{-1} are attributed to Si–OH of silica.[23] After pyrolyzing rGO@SS in high temperature argon to form nanocookies, the peak at 2820–2967 cm^{-1} disappeared due to the destruction of the aliphatic C–H structure of polystyrene, but other peak positions remained unchanged indicating a similar structure of nanocookie and rGO@SS except for polystyrene disapperance.

Further information on rGO and silica may be deduced from Raman spectra, Figure 3b. The peak at approximately 950 cm^{-1} is a phonon mode of silica,[24] which was seen in all the products except rGO. In contrast, in-phase sp^2 bond vibration of the graphite lattice (G band) at 1580 cm^{-1} and the disorder band caused by graphene edge functional group (D band) at 1350 cm^{-1} are characteristic of rGO present; such bands are present in all the products except PSS, which was pyrolyzed in air. The relative peak ratio of G/D is highest in rGO and progressively decreases from rGO@SS to nanocookie, which may be due to the blocking effect caused by covering the rGO surface with other species (larger disorder).[20,25]

When nanoparticle suspensions (in PBS) were irradiated by NIR (808 nm, 2 W cm^{-2}), a significant increase in temperature was found (**Figure 4a**) in the rGO (1 mg/mL), rGO@PSS (6.25 mg/mL) and nanocookie (6.15 mg/mL) suspensions, which all have nearly the same rGO content according to weight analysis. The temperature rise here was caused by nanoparticle absorption, since particle-free PBS (5.6 mg/mL) solution experienced no heating. In comparison with the solution of rGO, an excellent photon receptor, the rGO@PSS solution at the same rGO concentration has both a slower rate of temperature rise and a lower final temperature, but nanocookie solution and rGO solution behave almost the same. The different behavior cannot be due to different thermal conductivity (e.g., silica is a poorer thermal conductor than rGO), since thermal conductivity should only affect the transient but not the final, steady-state temperature, which is determined by photon absorbance. Such absorption is lower in rGO@PSS presumably because of some blocking effect (e.g., reflection or deflection) of silica. Remarkably, when silica (and polystyrene) is converted to the carbon-coated vertical cell-like structure in nanocookies, it apparently does not affect rGO-NIR interaction. Thus the same strong NIR absorbance is exhibited by both nanocookies and bare rGO.

The loading capacity of a model hydrophobic drug CPT is higher for nanocookie (0.878 mmol g^{-1}) than for rGO (0.433 mmol g^{-1}) and PSS (0.336 mmol g^{-1}) (Figure 4b). This difference cannot be due to the surface area alone, which is highest for PSS. Instead, it most likely reflects an affinity between CPT and carbonaceous surfaces, which nanocookies have in abundance. Non-graphitizing carbon layers are well known to possess a nanoporous structure and are potent absorbent of water-insoluble drugs.[26] Our drug release data are in support of this hypothesis. Figure 4c shows profiles of drug release from rGO-CPT, nanocookie-CPT, rGO@PSS-CPT and PSS-CPT in DMSO solution. While more than 80% of the CPT is released from PSS and rGO@PSS in 40 h, the release from rGO and nanocookie is insignificant.

Photon heating has a dramatic enhancement effect on drug release. In one experiment, we irradiated the solution by NIR during the first 5 min, and monitored the release amount continuously for 120 min.

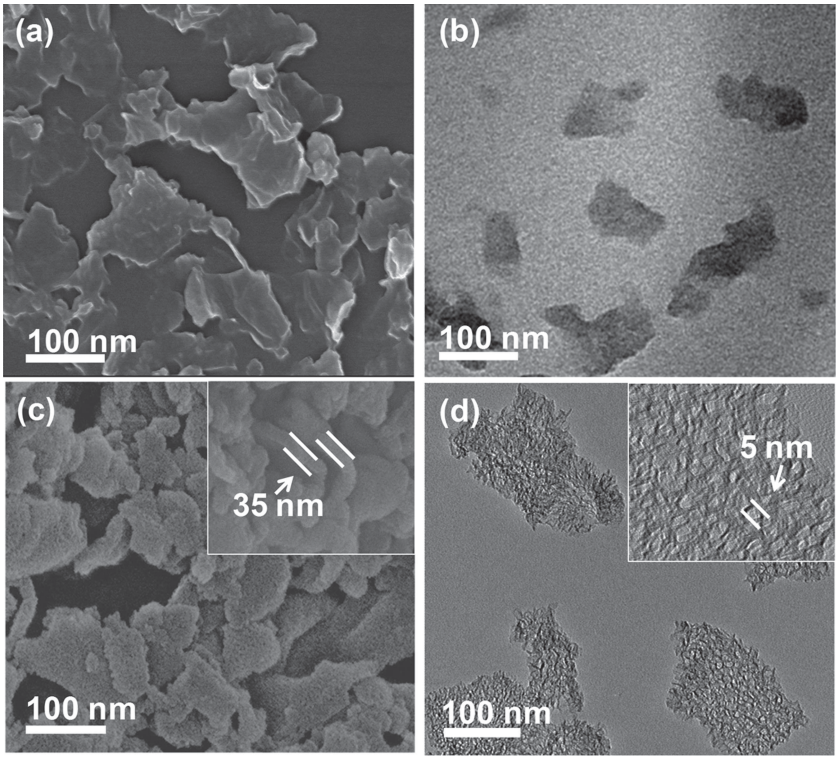

Figure 2. (a) FE-SEM and (b) low-magnification TEM images of rGO@SS; (c) FE-SEM and (d) low-magnification TEM images of nanocookies. Inset: High-magnification TEM image of a nanocookie.

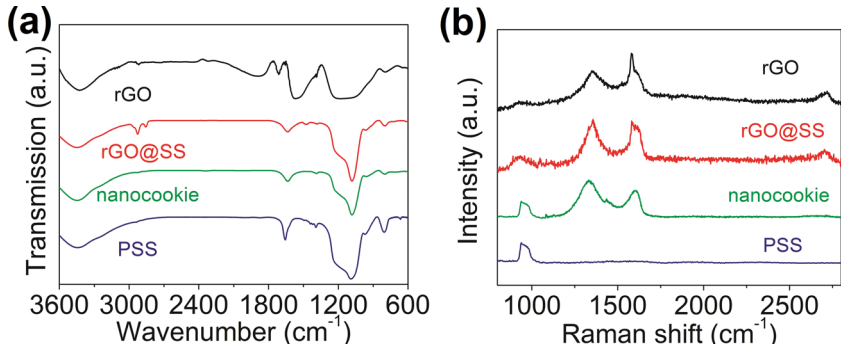

Figure 3. (a) FTIR and (b) Raman spectra of rGO, rGO@SS, nanocookie and PSS.

Both rGO and nanocookies showed a step-like initial release, but the release continued albeit at a much slower rate even after 5 min (Figure 4d, one exposure). In another experiment, another 5 min exposure was given after a waiting time of 5 min, and the sequence of irradiation/waiting was repeated 5 times. In this case, nanocookies showed repeated step-like release but rGO did not (Figure 4d, multiple exposures). After multiple exposures, the cumulative drug release from nanocookies reached 90% whereas that of rGO was only 22%. This difference may suggest that the π–π stacking interaction between CPT drug molecules and rGO is stronger than the noncovalent interaction between CPT and nanocookie,[24] as schematically illustrated in Figure S1 in the Supporting Information. While stimulating drug release from rGO and nanocookie, NIR irradiation has no apparent effect on the structure of CPT. This was verified by UV–vis spectra which were identical before and after irradiation (Figure S2 in Supporting Information).

To track intracellular uptake, we labeled rGO and nanocookies using a red fluorescent dye Rhodamine B (RhoB) with silane conjugation chemistry. After incubating MDA-MB 231 cells with rGO-RhoB or nanocookie-RhoB for 4 h, we stained cytoskeletons green with phalloidin, and nuclei blue with DAPI (see **Figure 5**). The composite image for the nanocookie-RhoB group in Figure 5b shows higher nanoparticle (red) intensity within the cells than that of the rGO-RhoB group in Figure 5a, showing mostly nanoparticles at cell surfaces. The nanocookie-RhoB was internalized into cells as demonstrated by confocal image and flow cytometry after 4 h incubation, showing in

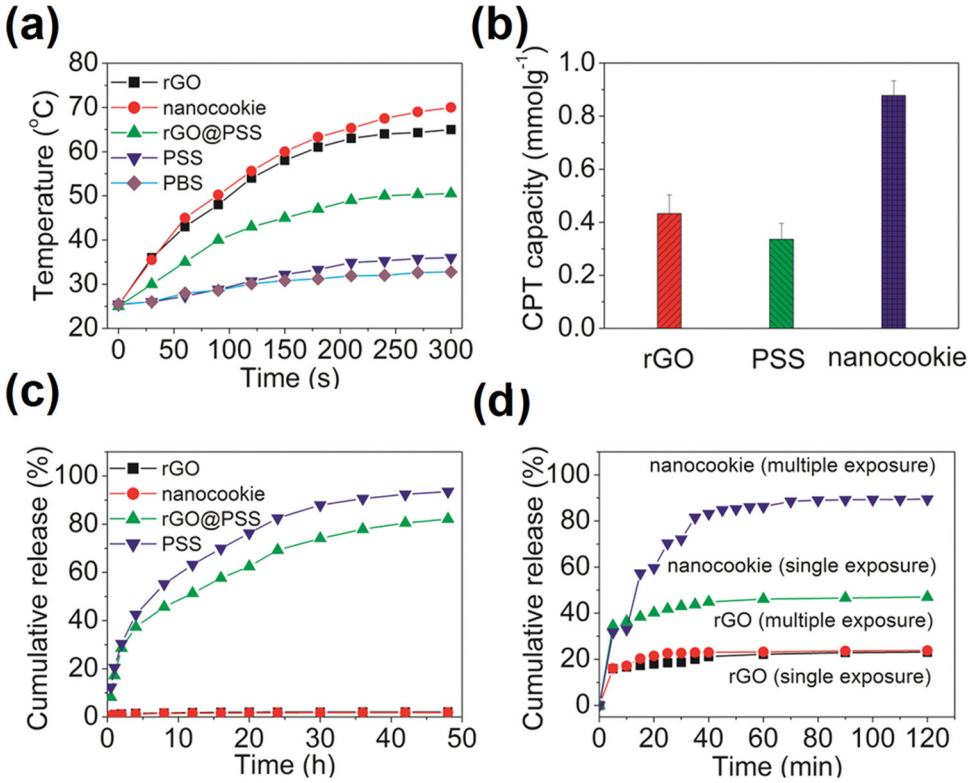

Figure 4. (a) Heat-generation kinetics of PBS suspension of rGO, nanocookie, rGO@PSS, PSS, and control (PBS), under NIR (808 nm, 2 Wcm^{-2}) exposure initiated at time 0. Nearly the same amount of rGO (per measurement of weight loss after burning was used in rGO (1 mg/mL), rGO@PSS (6.15 mg/mL) and nanocookie (6.25 mg/mL). The amount of silica was nearly the same in nanocookies and PSS. (b) CPT loading in rGO, PSS and nanocookie. (c) Natural drug (CPT) release profiles from rGO, nanocookie, rGO@PSS, and PSS. (d) NIR-stimulated drug (CPT) release profiles from rGO and nanocookie: single 5 min NIR exposure initiated at time 0, multiple exposures repeated 5 times after 5 min waiting time following previous exposure.

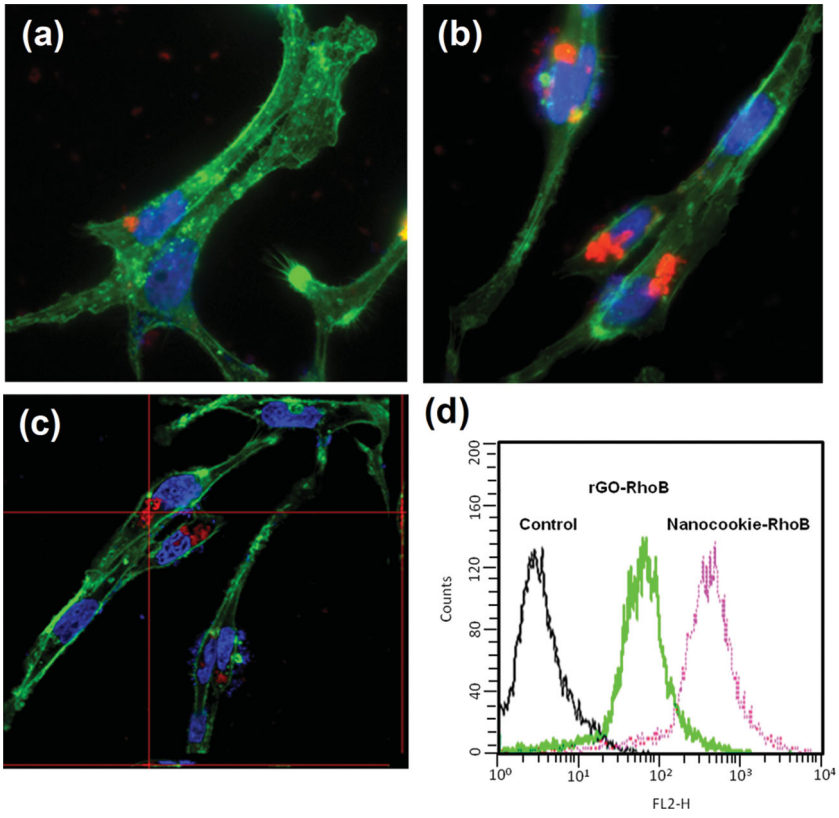

Figure 5. Fluorescence images of MDA-MB-231 cells incubated with DMEM solution of rGO-RhoB (a) and nanocookie-RhoB (b) for 4 h at 37 °C. Blue, red and green fluorescence represent nucleus staining with DAPI, nanoparticle staining with RhoB andcytoskeleton staining with phalloidin. (c) shows confocal images of multiple cross sections exhibiting various locations of nanocookie-RhoB within cells. (d) Flow cytometry analysis of rGO-RhoB and nanocookie-RhoB in MBA-MD231 cells after incubation for 4 h. Control: cells incubated without nanoparticles.

Figure 5c and Figure 5d, respectively. Both nanocookie-RhoB and rGO-RhoB cells show fluorescence, but the fluorescence intensity (the horizontal axis) of the former is much higher. Therefore, the additional carbon-silica construct on nanocookie can significantly enhance cell uptake.

In vitro photothermal therapy study was conducted on MDA-MB 231 cells (a human breast cancer cell line) incubated with control group (PBS only), nanocookie–CPT, CPT-free nanocookies, and free CPT drug. After 4 h incubation, cells were NIR irradiated (2 W cm^{-2}) for periods from 0 to 5 min, then stained with propidium iodide to characterize cell viability: live cells appeared green, dead cells appeared red (**Figure 6**a). Quantification of these results as percent cell viability is provided in Figure 6b. It shows no cell kill by NIR alone (control), and most kill by NIR and- nanocookie-CPT combined in a (irradiation) dose-dependent manner: at the end of 5 min irradiation, 90% cell kill was achieved. Importantly, CPT-free nanocookies when administered with NIR also caused some cell kill in a dose-dependent manner, confirming the photothermal effect. Meanwhile, without irradiation, nanocookie–CPT providing only chemotherapy caused less cell kill than CPT-free nanocookies providing only photothermal therapy. For control, free CPT showed a relatively small chemotherapy effect. Here, the (free) CPT concentration (in PBS) is 1 μM which is actually slightly higher than the (nanocookie-bound) CPT concentration (0.878 μM) used in the nanocookie–CPT solution.

In vivo tumor treatment was conducted in nude mice bearing MDA-MB 231 tumor cells. Before treatment, the tumor size was approximately 153 mm^3. The nanocookie and nanocookie–CPT solution (100 mg/L, 100 μL) was then injected by intravenous injection to achieve a dosage of 5 mg/kg per mouse body weight. NIR irradiation (2 W cm^{-2}) was initiated 24 h post injection and lasted for 5 min during which the temperature in the tumor increased from 31 °C to 60 °C. For control, mouse injected with PBS was also irradiated but showed no temperature increase. The size of tumor decreased in nanocookie and nanocookie-CPT treated mouse but increased in the control mouse confirming the therapeutic effect. Indeed, the tumor in thus treated mouse apparently disappeared 14 days post treatment, and did not reappear again in the 2 months after that(data not shown here). Because the temperature (60 °C) from thermal effect of nanocookie is high enough to kill tumor alone, in this experiment it is hard to distinguish the main contribution of tumor killing effect from thermal-therapy or chemotherapy. To further demonstrate that the nanocookie–CPT–NIR treatment is superior to chemotherapy or NIR treatment alone, and that nanocookie is essential for achieving superiority, tumor bearing mice were made to receive the following treatments, PBS+NIR (control), CPT+NIR (combine treatment without nanocookies), nanocookie-CPT, nanocookie+NIR and nanocookie–CPT+NIR. (Intravenous injection was used and NIR treatment was provided at a low power density, 0.75 W/cm^2) As shown in **Figure 7**, the surface temperature of tumor in nanocookie+NIR and nanocookie–CPT+NIR treated mice reached 50–53 °C, but that on PBS+NIR and CPT+NIR treated mice barely rose to 38–39 °C (Figure 7a). (There was no temperature change in nanocookie–CPT treated mice, which did not receive NIR.) The tumor appearance on the mice treated with nanocookie+NIR and nanocookie–CPT+NIR was that of a black scab, but no change in appearance was apparent in other groups (Figure 7b). Throughout the first 14 days post treatment, the size of tumor decreased in nanocookie+NIR and nanocookie–PT+NIR treated mice, but it increased in other treatments (Figure 7c). After 14 days, the tumor size of nanocookie+NIR treated mice began to increase again, but in nanocookie-CPT + NIR treated mice the size continued to decrease and the tumor eventually disappeared after 30 days (Figure 7c). Meanwhile, there was no noticeable body weight loss after various treatments (Figure 7d). These results confirmed the synergistic effect of nanocookie–CPT+NIR, compared to CPT and NIR alone, and to CPT+NIR but without nanocookies.

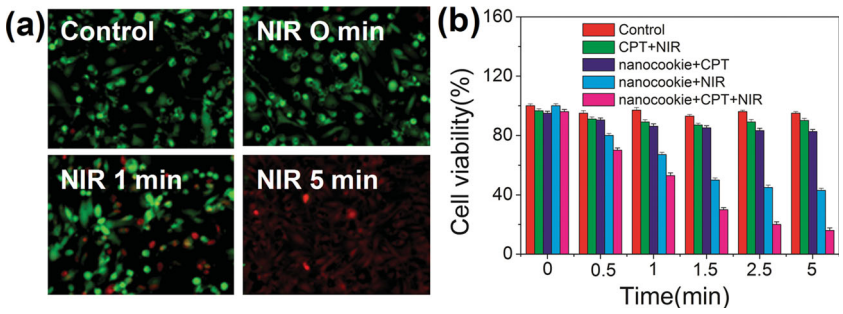

Figure 6. (a) Fluorescent images of MDA-MB-231 cells: cells incubated without nanocookie–CPT as control compared with cells incubated with nanocookie-CPT and NIR treatment for 0 min, 1 min, and 5 min. Green fluorescent cells are live ones, red fluorescent cells are dead or compromised ones. (b) Quantitative cell viability from cell counting. Five fields of view were counted per slide; each treatment was performed in triplicate.

One concern for using any new carrier is its potential toxicity *in vivo*. Although biocompatibility with human cells has been reported for graphene oxide (GO) based nanomaterials, their potential in vivo toxicity has also been noted.[14,27] For example, GO was found to accumulate in lung in a relatively larger amount than in other organs,[28] and to cause remarkable thrombus after intravenous injection,[29] which might be attributed to its positive surface charge.[30] Therefore, a biodistribution study was conducted by intravenous injection of nancookie–CPT followed by NIR treatment to tumor bearing mice. (Fluorescent CPT-cy5.5 was used for this study; injection used the dosage, 5 mg/kg; NIR irradiation at 0.75 W/cm^2 with the same protocol as before.) As shown in Figure S3a in the Supporting Information, major organs were collected from sacrificed mice 2 h, 24 h and 48 h post treatment and examined by fluorescence spectroscopy. At first 2 h, the fluorescence intensity of all organs and tumor was weak indicating most of nanocookie–CPT was transported in the blood circulation. Nanocookie-CPT was mainly trapped by reticuloendothelial system (RES) 24 h post treatment. After 24 h administration, fluorescence intensity of liver, spleen and kidney apparently decreased suggesting nanocookie-CPT was excreted gradually from those organs. In contrast, considerable fluorescence intensity still remained with the tumor 48 h post treatment suggesting continued retention of nanocookies, which is consistent with reports that nanoparticles (nanocookies) can be taken up by tumor vasculature through enhanced permeability and retention (EPR) effect.[31,32] Therefore, intravenous injection is an effective method to deliver nanocookies, which show no abnormal accumulation at sites other than tumor.

Lastly, tissues of the same mice receiving intravenous injection of nanocookie–CPT and NIR treatment were histologically analyzed. Hematoxylin and eosin (H&E)-stained tissue slices from major organs (heart, lung, liver, spleen and kidney) obtained 7 day post treatment showed no noticeable sign of damage (Figure S4a in the Supporting Information), suggesting

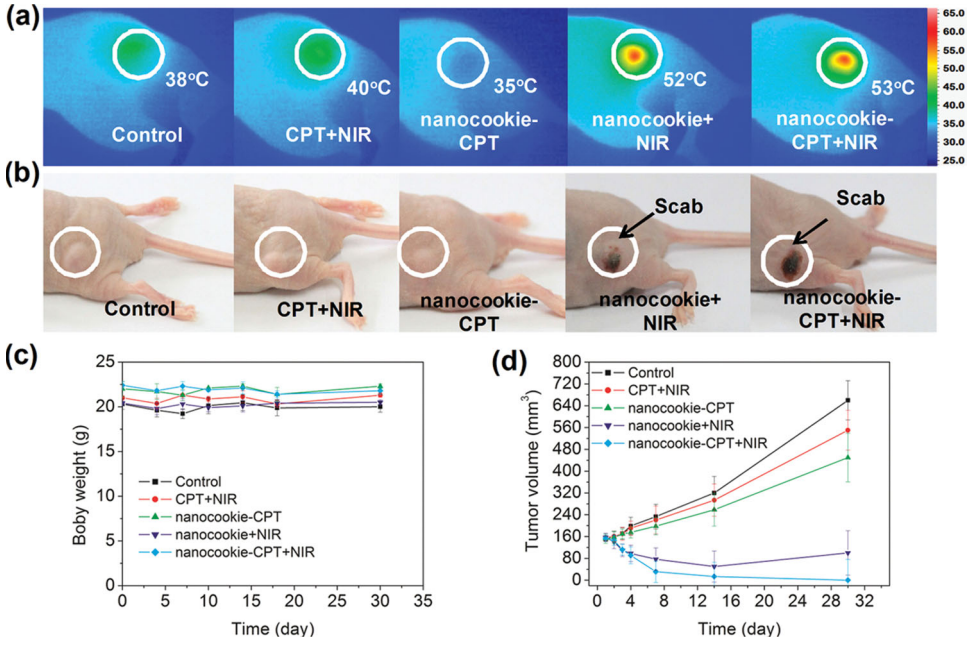

Figure 7. MDA-MB231 tumor-bearing nude mouse, tumor site indicated by arrow. (a) infrared thermal image of PBS+ NIR (Control), CPT+NIR, nanocookie–CPT (no NIR), nanocookie+NIR, nanocookie–CPT+NIR treatment. Color bar on right shows temperature in degrees Celcius. (b) At day 4 after NIR irradiation (808 nm, 0.75 Wcm^{-2}, 5 min, 1 min interval for every min treatment). Tumor turned into a scab at sites injected with nanocookie+NIR and nanocookie-CPT+NIR. (c) Tumor volume change after PBS+ NIR (Control), CPT+NIR, nanocookie–CPT (no NIR), nanocookie+NIR, nanocookie–CPT+NIR treatment.(d) Body weight of PBS+ NIR (Control), CPT+NIR, nanocookie-CPT (no NIR), nanocookie+NIR, nanocookie–CPT+NIR treatment group showing no change. Injection dosage: 5 mg/kg. white circles in (a) and (b) represent tumor site.

no severe toxicity of the nanocookie–CPT+NIR treatment to non-tumor sites. In contrast, in tumor slices taken from both nanocookie+NIR and nanocookie–CPT+NIR treated mice, large areas of dead cells without nuclei were found (Figure S4b). Meanwhile, under other treatments not involving nanocookies plus NIR, many nuclei still existed in the tumor slices. A further comparison of the large nuclei-free area (indicating tumor cell kill) confirmed that the synergistic thermal and chemotherapeutic effects (nanocookie–CPT+NIR) are more effective than thermal effect alone (nanocookie+NIR) and chemotherapy alone (nanocookie+CPT). Therefore, direct histological evidence has corroborated our tumor size measurements in vivo (Figure 7c) and cell viability data in vitro (Figure 7b) concerning the efficacy of nanocookie-CPT+NIR treatment. It has also confirmed our biodistribution observations (Figure S3) that nanocookie-based drugs seem to have at most benign side effects on non-tumor sites.

3. Conclusions

In summary, a one-pot, scalable synthesis method has been developed for a new class of photosensitive inorganic nanocomposite that emulates liposomes with combined hydrophilic/hydrophobic properties and excellent biocompatibility. The nanocomposite contains reduced graphene oxide, amorphous carbon, and mesoporous silicon, which endow unique attributes of photon-thermal conversion, drug absorption, and cell compatibility/penetrability, respectively. Tthe nanocomposite allows high-efficiency cell uptake by MDA-MB231 cells and provides a large payload for hydrophobic drug, (S)-(+)-camptothecin. Although nanocookie–CPT will have high accumulation in liver after 24 h tratment, With this nanocomposite, combined, NIR-triggered, localized drug release and photothermal therapy have been demonstrated, in vitro and in vivo, with a remarkable cancer cell killing effect and no significant side-effect to normal cell. Such nanoplatforms with built-in capabilities for triggerable fast-response and combined hyperthermia chemotherapy are expected to open a new avenue for cancer treatment, possibly leading to clinical applications.

4. Experimental Section

Materials: (S)-(+)camptothecin (CPT), cetyltrimethylammonium bromide (CTAB), ethanol (99.5%), *n*-octane,2,2′-azobis(2-amidinopropane) dihydrochloride (AIBA), and lysine were purchased from Aldrich. Tetraethylorthosilicate (TEOS) was purchased from Merck. Rhodamine B and graphite powder (325 mesh) were purchased from Alfa Aesar. LIVE/DEAD Viability/Cytotoxicity Kit and Alexa Fluor 488 Phalloidin were purchased from life technologies(United state).

Synthesis of Small-Sized rGO: The rGO was prepared by a modified Hammer method, as described by Zhijun Zhang et al.[17] The first step is to obtain graphene oxide (GO). In brief, native graphite flakes were preoxidized by mixing with H_2SO_4, $K_2S_2O_8$, and P_2O_5 and incubated at 80 °C for 12 h. After washing with distilled water (DI water) and ethanol until neutral, the flakes were dried overnight in an oven under nitrogen. Subsequently, the preoxidized graphite powder was further oxidized by placing in H_2SO_4 at 0 °C and adding $KMnO_4$ slowly with stirring. The mixture was continuously stirred in an ice bath for 2 h before the reaction was terminated with distilled water. To remove MnO_2, as described by Kovtyukhova et al.,[33] H_2O_2 was added until the mixture color changed to bright yellow. The collection and purification of the graphite oxide powder was carried out by the addition of HCl (1%) and centrifugation at 6000 rpm for 5 min, followed by washing 3 times with an excess of distilled water until pH 6–7 was achieved. Then, the precipitate was redispersed in distilled water. An ultrasonic probe was used to exfoliate the oxidized graphite, and the resulting small-size GO was collected from the supernatant by centrifugation at 12 000 rpm for 30 min. The supernatant (GO content: 3 mg/mL, pH 6–7) did not precipitate over several months. To obtain rGO, the dispersion of GO was added to dilute ammonia solution to adjust the solution to pH 11.5–11.8, and then, the solution was heated in an oil bath at 80 °C for 12 h. After reduction of the GO (the color of the solution turned from brown to black), the rGO aggregates were sonicated for 1 h to exfoliate the rGO sheet stacks to become a stable colloidal solution. To obtain the small-sized rGO, the dispersion was centrifugated at 12 000 rpm for 30 min to remove the precipitates of large-size rGO sheets, while the supernatant was kept. The small-size rGO sheets were in the supernatant. The dispersion (rGO content: 1.2–1.5 mg/mL, pH 11.3–11.4) maintained a stable state for several months.

Synthesis of Nanocookies: An amount of 300 mg CTAB was dissolved in a mixture of 30 mL octane and 96 ml rGO dispersion (0.27–0.3 mg/mL) at 70 °C. (CTAB was adsorbed to the rGO surface, increasing its zeta potential from -22 mV to +31 mV.) After stirring for 20 min, 6.5 mL styrene monomer, 66 mg lysine, 300 mg TEOS, and 115 mg AIBA were added to the system and stirred for 4 h. After that, the suspension was allowed to cool naturally to room temperature. The gray powder was collected by centrifugation at 5000 rpm for 10 min, followed by washing 3 times with an excess of pure ethanol and drying in a vacuum at 60 °C. For sulfonation of polystyrene as describe by Gibson et al.,[34] the gray powder was soaked in H_2SO_4 solution at 40 °C for 4 h, followed by washing 3 times with an excess of pure ethanol and drying in a vacuum at 60 °C. Finally, the sulfonated-polystyrene was completely carbonized by heat treatment at 800 °C for 3 h under argon gas to obtain nanocookies. Other products (PSS, rGO@SS and rGO/PSS) were similarly obtained following a slight variation of the above procedure as indicated in Figure 2a and b.

Loading (S)-(+)-Camptothecin (CPT) into Drug Carriers: To load the drug, different carriers were first soaked in a solution containing 5 mg CPT and 3 mL DMSO, followed by stirring for 24 h, as described by Lu et al.[35] The drug-loaded carrier was dried under vacuum to remove DMSO, then washed 3 times with phosphate buffered saline (PBS, pH 7.4) solution to remove weakly absorbed CPT. The amount of loaded drug was calculated using the difference in concentration of the drugs in PBS (pH 7.4) before and after loading, determined by UV-vis spectroscopy (8453 UV-visible spectrophotometer, Agilent Technologies, US) using the absorption peak of 366 nm (the I_{max} of free CPT).

Drug Release Test: Natural drug release profiles of different drug loaded carriers in 10 mL DMSO solution were determined at room temperature. For quantitative measurement, we set the total CPT amount in the nanocarriers before release as 100%. 2 mlLDMSO solution with dispersed drug-loaded carrier was removed and separated by centrifugation at 5000 rpm for 10 min. The collected supernatant was a clear solution without carrier. The amount of CPT was characterized using the absorption peak of 366 nm with UV–vis spectroscopy. NIR-stimulated drug release was similarly determined with different NIR treatment times.

In vitro Cell Uptake and Cytotoxicity: MDA-MB-231 (a human breast cancer cell) was maintained in DMEM (Dulbecco's modified Eagle's medium) containing 10% fetal bovine serum, 100 units/mL penicillin, and 100 μg/mL streptomycin. Cells were cultured with the complete medium at 37 °C in a humidified atmosphere of 5% CO_2 in air. In vitro cytotoxicity of nanocookies to MDA-MB-231 was tested using an in vitro proliferation method with MTT. In brief, 1×10^4 cells were plated onto 96-well plates for cellular attachment. The cells were then exposed to the growth medium of nanocookies at 37 °C. After incubation, 20 μL of MTT solution was added, and the cells were incubated for an additional 4 h. The medium was then replaced with 100 μL of DMSO, and the absorbance was monitored using a sunrise absorbance microplate

reader at dual wavelengths of 570 nm and 650 nm. To investigate the cellular uptake of rGO and nanocookies with fluorescene imaging by mixing RhoB solution with rGO and nanocookies, then stirring magnetically for 24 h. After 24 h, the unbound Rho B was removed by centrifuging at 6000 rpm for 15 min and washing 3 times with PBS solution (pH 7.4). Then, MDA-MB-231 was incubated with rGO-RhoB (100 μg/mL) and nanocookie-RhoB (100 μg/mL) for 4 h. The cells were observed with an inverted Nikon microscope (TE-2000U, Nikon, Japan) and a confocal microscope (Nikon, C1).

In vitro Live/Dead Cell Imaging After NIR Irradiation: MDA-MB 231 cells grown in 6-well tissue culture plates for 48 h were incubated for 4 h with nanocookie–CPT by dispersing in growth medium. Subsequently, the MDA-MB 231 tumor cells mixed with nanocookie–CPT were washed two times with PBS solution to remove the excess nanocookie-CPT. Then, the cells were floated from the culture plate by adding trypsin and distributed in a 100 μL cells/ nanocookie-–PT suspension onto 96-well tissue culture plates, followed by exposure to NIR light (808 nm, 2 W cm^{-2} as measured at the sample). Following 5min irradiation, the cells were stained using a LIVE/DEAD kit, following manufacturer's instructions.

In vivo combined chemo-photothermal therapy: An optical-fiber-coupled 808 nm high-power laser diode was used to irradiate tumors. Before photothermal therapy, we injected a suspension of nanocookie–CPT (5 mg/kg) by intravenous injection. The other control groups were treated with same protocol as nanocookie–CPT. The tumor on each nude mouse was irradiated with NIR at a power density of 0.75 W cm^{-2} for 5 min. To avoid excessive heat damage, irradiation was administered intermittently as follows: 60 s on/10 s off, repeated five times. The tumor sizes were measured with a caliper every other day and volumes were calculated as (tumor length) × (tumor width)^2/2. The relative tumor volumes were calculated as V/V_0 (where V_0 is the tumor volume when the treatment was initiated).

Fluorescent lLabeling of Nanocookie–CPT: To graft fluorescent dye, Cy5.5, nanocookie–CPT was reacted with 3-aminopropyl)triethoxysilane (ATPMS) in a pH 7.4 PBS solution. The reaction was reacted overnight at room temperature while avoiding light. After overnight reaction at room temperature, the unbound ATPMS with nanocookie-CPT sample was removed by centrifuging at 10 000 rpm for 15 min and washing 3 times with PBS solution (pH 7.4). the nanocookie–CPT–ATPMS reacted with fluorescent dye, Cy5.5, via EDC/NHS coupling method overnight at room temperature. After reaction, unbound Cy5.5 EDC and NHS molecules were removed by centrifuging at 12 000 rpm for 15 min and washing 3 times with PBS solution (pH 7.4).

In vivo Fluorescence Imaging: Nanocookie–CPT–Cy5.5 nanoparticles were injected into MDA-MB 231 tumor bearing nude mice by tail vein. Fluorescent images were recorded by IVIS Spectrum (IVIS imaging System 200 Series, Caliper Life Science, USA). Living Image software Version 3.0 (Xenogen) was used to acquire and quantify the fluorecence. After 2, 24, and 48 h post injection, mice were sacrificed to collect tumor and major organs, including heart, lung, liver, spleen and kidney, from which the fluorescence images of tumor and major organs were obtained (Cy5.5 channel, ex = 615–665 nm, em = 695–770 nm).

Histology Analysis: Mice with various treatments (without any injection (control), CPT-NIR, nanocookie–CPT, nanocookie+NIR and nanocookie–CPT+NIR) were sacrificed 7 days post treatment by CO_2 asphyxiation for necropsy. Tumor and major organs including heart, lung, liver, spleen, kidneys, and spleen were collected, fixed in 10% neutral buffered formalin for 12 h, processed into paraffin, and sectioned into slices. After staining with hematoxylin and eosin (H&E), they were examined by a digital microscope (TE-2000U, Nikon, Japan).

Supporting Information

Supporting Information is available from the Wiley Online Library or from the author.

Acknowledgements

This work was financially supported by the National Science Council of the Republic of China, Taiwan under Contracts NSC 100-2320-B-009-006-MY2 and NSC 99-2221-E-009-070-MY3, and by the "Aim for the Top University" program of the National Chiao Tung University and the Ministry of Education, Taiwan, R.O.C. I.-W. Chen acknowledges support from Army Medical Research & Material Command Grant No. W81XWH-10-1-0320 and W81XWH-10-1-0604.

Received: May 23, 2013
Published online: August 23, 2013

[1] W. Gao, J. M. Chan, O. C. Farokhzad, *Molecular Pharmaceut.* **2010**, *7*, 1913.
[2] H. Dai, Q. Chen, H. Qin, Y. Guan, D. Shen, Y. Hua, Y. Tang, J. Xu, *Macromolecules* **2006**, *39*, 6584.
[3] J. Liu, Y. Pang, W. Huang, Z. Zhu, X. Zhu, Y. Zhou, D. Yan, *Biomacromolecules* **2011**, *12*, 2407.
[4] K. Hayashi, K. Ono, H. Suzuki, M. Sawada, M. Moriya, W. Sakamoto, T. Yogo, *ACS Appl. Mater.Interfaces* **2010**, *2*, 1903.
[5] K. W. Ferrara, M. A. Borden, H. Zhang, *Acc. Chem. Res.* **2009**, *42*, 881.
[6] Q. Yuan, Y. Zhang, T. Chen, D. Lu, Z. Zhao, X. Zhang, Z. Li, C.-H. Yan, W. Tan, *ACS Nano* **2012**, *6*, 6337.
[7] J. L. Vivero-Escoto, I. I. Slowing, B. G. Trewyn, V. S. Y. Lin, *Small* **2010**, *6*, 1952.
[8] A. Schlossbauer, J. Kecht, T. Bein, *Angew. Chem. Int. Ed.* **2009**, *48*, 3092.
[9] R. Liu, Y. Zhang, X. Zhao, A. Agarwal, L. J. Mueller, P. Feng, *J. Am. Chem. Soc.* **2010**, *132*, 1500.
[10] H. P. Rim, K. H. Min, H. J. Lee, S. Y. Jeong, S. C. Lee, *Angew. Chem. Int. Ed.* **2011**, *50*, 8853.
[11] S.-H. Hu, Y.-W. Chen, W.-T. Hung, I. W. Chen, S.-Y. Chen, *Adv. Mater.* **2012**, *24*, 1748.
[12] J. T. Robinson, S. M. Tabakman, Y. Liang, H. Wang, H. S. Casalongue, V. Daniel, H. Dai, *J. Am. Chem. Soc.* **2011**, *133*, 6825.
[13] W. Zhang, Z. Guo, D. Huang, Z. Liu, X. Guo, H. Zhong, *Biomaterials* **2011**, *32*, 8555.
[14] K. Yang, J. Wan, S. Zhang, B. Tian, Y. Zhang, Z. Liu, *Biomaterials* **2012**, *33*, 2206.
[15] H. Hatakeyama, H. Akita, H. Harashima, *Adv. Drug Deliv. Rev.* **2011**, *63*, 152.
[16] O. Akhavan, E. Ghaderi, S. Aghayee, Y. Fereydooni, A. Talebi, *J. Mater. Chem.* **2012**, *22*, 13773.
[17] Z. Liming, X. Jingguang, Z. Qinghuan, L. Liwei, Z. Zhijun, *Small* **2010**, *6*, 537.
[18] W. S. Hummers Jr, R. E. Offeman, *J. Am. Chem. Soc.* **1958**, *80*, 1339.
[19] Z.-M. Wang, W. Wang, N. Coombs, N. Soheilnia, G. A. Ozin, *ACS Nano* **2010**, *4*, 7437.
[20] P. Valle-Vigon, M. Sevilla, A. B. Fuertes, *Chem. Mater.* **2010**, *22*, 2526.
[21] A. S. Patole, S. P. Patole, H. Kang, J.-B. Yoo, T.-H. Kim, J.-H. Ahn, *J. Colloid Interface Sci.* **2010**, *350*, 530.
[22] E.-Y. Choi, T. H. Han, J. Hong, J. E. Kim, S. H. Lee, H. W. Kim, S. O. Kim, *J. Mater. Chem.* **2010**, *20*, 1907.
[23] R. Tian, O. Seitz, M. Li, W. Hu, Y. J. Chabal, J. Gao, *Langmuir* **2010**, *26*, 4563.
[24] Y. D. Glinka, M. Jaroniec, *J. Appl. Phys.* **1997**, *82*, 3499.
[25] K. N. Kudin, B. Ozbas, H. C. Schniepp, R. K. Prud'homme, I. A. Aksay, R. Car, *Nano Lett.* **2008**, *8*, 36.
[26] A. Kumar, R. F. Lobo, N. J. Wagner, *Carbon* **2005**, *43*, 3099.

[27] K. Yang, H. Gong, X. Shi, J. Wan, Y. Zhang, Z. Liu, *Biomaterials* **2013**, *34*, 2787.
[28] K. Yang, J. Wan, S. Zhang, Y. Zhang, S.-T. Lee, Z. Liu, *ACS Nano* **2011**, *5*, 516.
[29] S. K. Singh, M. K. Singh, M. K. Nayak, S. Kumari, S. Shrivastava, J. J. A. Gracio, D. Dash, *ACS Nano* **2011**, *5*, 4987.
[30] S. K. Singh, M. K. Singh, P. P. Kulkarni, V. K. Sonkar, J. J. A. Gracio, D. Dash, *ACS Nano* **2012**, *6*, 2731.
[31] H. Maeda, J. Wu, T. Sawa, Y. Matsumura, K. Hori, *J. Control. Release* **2000**, *65*, 271.
[32] L. Jie, M. Liong, L. Zongxi, J. I. Zink, F. Tamanoi, *Small* **2010**, *6*, 1794.
[33] N. I. Kovtyukhova, P. J. Ollivier, B. R. Martin, T. E. Mallouk, S. A. Chizhik, E. V. Buzaneva, A. D. Gorchinskiy, *Chem. Mater.* **1999**, *11*, 771.
[34] H. W. Gibson, F. C. Bailey, *Macromolecules* **1980**, *13*, 34.
[35] J. Lu, M. Liong, J. I. Zink, F. Tamanoi, *Small* **2007**, *3*, 1341.